Supplementary Information

Topology-dependent temporal memory in coupled oscillator networks

Author: Yousef Jamali.

This supplementary file accompanies Topology-dependent temporal memory in coupled oscillator networks.

S1. Reproducibility and frozen validation design

The new independent replication contains 30 graph–frequency pairs, each comprising one Watts–Strogatz graph ($N = 128$, $k = 14$, rewiring probability 0.2) and its degree-preserving rewired counterpart (5 swaps per original edge). Both members of each pair use the same natural frequency vector. No graph or frequency seed is reused from the previously reported eight-pair exploratory dataset.

The design parameters are written in data/design_frozen.json and the full source in new_validation.py. Calibration uses only a training-noise sequence with 3,600 Euler–Maruyama time steps, 1,000 discarded steps, and seven coupling bisection evaluations in $[1.05, 2.60]$; it chooses the evaluation giving smallest training mismatch in mean global order. The first member always uses $K = 1.9$. Two new noise realizations for each condition have 6,000 steps, 1,800 discarded steps and every-fourth-step recording. Their values are averaged at the *graph pair* level before any paired inference. No holdout noise enters the K tuning.

S2. Definition and numerical verification of q

For m structural edges and $\acute{m} = \binom{N}{2} - m$ nonedges, $q = \acute{f}_E - \acute{f}_{\neg E}$ with $f_{ij} = \cos(\theta_i - \theta_j)$.

Equivalently, writing $p = m / \binom{N}{2}$, sum $s_E = \sum_{\{i,j\} \in E} \cos(\theta_i - \theta_j)$, and sum $s_{all} = (N^2 r^2 - N)/2$,

$$q = \frac{s_E}{m} - \frac{s_{all} - s_E}{\acute{m}}.$$

The production implementation evaluates q from sparse graph adjacency. The independent check in numerical_checks.py verifies it against direct evaluation of every edge and nonedge for small random graphs, as well as checking Euler–Maruyama steps directly against the simulated state equations.

The normalized autocorrelation estimate uses $\sum_t (q_t - \acute{q})(q_{t+k} - \acute{q}) / \sum_t (q_t - \acute{q})^2$ without a lag-dependent variance normalization. τ_q is its linearly interpolated first crossing of $1/e$ and differs conceptually from integrated correlation time. All 60 holdout trajectories in each graph condition yielded a finite first crossing within the 24-time-unit evaluation range.

S3. Full graph-level independent validation

The mean τ_q was 2.1782 for original graphs and 1.1594 for rewired graphs; graph-level paired difference 1.0188 (95% percentile bootstrap interval 0.5412–1.7136). Twenty-seven of 30 independent pair differences were positive (two-sided sign test $p = 8.43 \times 10^{-6}$). The median graph-paired difference was 0.6269, showing that the mean is affected by some large positive differences. A 10,000-draw bootstrap resamples entire graph pairs, not individual time frames or noise realizations.

After within-trajectory regression on $1, r^2(t), r^4(t), r^2(t-\Delta), r^2(t-2\Delta)$ with $\Delta = 0.2$, the mean residual q crossing time was 1.1810 for original versus 0.9016 for rewired graphs. The paired difference was 0.2794 (95% bootstrap interval 0.2141–0.3573; 29/30 positive, two-sided sign-test $p = 5.77 \times 10^{-8}$). These are *descriptive residuals*: the regression does not ensure independence of global synchronization history or nonlinear dynamical coupling.

The mean r was 0.3952 and 0.3940, respectively, with paired difference 0.0012 (95% interval −0.0123 to 0.0134). Its standard deviation was 0.1049 and 0.0856, a systematic difference despite mean matching. The graph-level mean of within-pair Wasserstein distances between empirical r distributions was 0.0359. The original/rewired distribution of r cannot be claimed fully matched. Analyses therefore address temporal memory conditional on *approximately matched mean* order parameter, not a fully controlled order-parameter process.

The calibrated K in rewired graphs ranged from 1.232 to 2.213. The training absolute mismatch in mean r had median 0.0038 and maximum 0.0317. In a sensitivity study restricted to 12 pairs, memory of rewired graphs did not exhibit a sudden reversal when K was perturbed by ±0.08, although responses to K were not negligible (main Fig. 2).

S4. Integration step check

Eight independent graph pairs were reintegrated at $dt = 0.05$ and $dt = 0.025$ using a common Brownian path constructed from summed adjacent fine increments. At coarse and fine steps, mean original-versus-rewired q memory differences were 1.213 and 1.607, respectively. Synchronization-adjusted memory differences were 0.370 and 0.333, respectively. These comparisons support preservation of the direction of the effect; they do not establish complete convergence of the crossing-time estimator and involve only eight networks. See data/step_halving.csv and Supplementary Fig. S2.

S5. Derivation of the spectral relation

Let $L = U \Lambda U^{\top}$ be the Laplacian and $z_i = e^{i\theta_i}$. The identity $z^* L z = 2m - 2 \sum_{(i,j) \in E} \cos(\theta_i - \theta_j)$ and the all-pairs relation yield

$$q = 1 + \frac{N+2m}{2\acute{m}} - \frac{N}{2\acute{m}}\left|a_1\right)^2 - \left(\frac{1}{2m} + \frac{1}{2\acute{m}}\right)\sum_{a=2}^{N} \lambda_a \left|a_a\right)^2 .$$

This identity is exact for all phases and does not imply a closed dynamics for $\left|a_a\right)^2$. In the near-locking identical-frequency approximation, the transverse modes x_a are independent stationary Ornstein–Uhlenbeck processes satisfying $d\,x_a = -\gamma_a x_a\,dt + \sqrt{2D}\,dW_a$, $\gamma_a = K\lambda_a / \langle k \rangle$, $Var(x_a) = c_a = D/\gamma_a$. The quadratic contribution $q - Eq = \sum_{a=2}^{N} b_a\left(x_a^2 - c_a\right)$ implies by Gaussian fourth moments

$$C_q(\tau) = 2\sum_{a=2}^{N} b_a^2 c_a^2 e^{-2\gamma_a|\tau|} .$$

The corresponding normalized ACF is reported in the main text. The heterogeneous phase-locked extension uses the weighted Laplacian of $A_{ij}\cos\left(\theta_i^* - \theta_j^*\right)$ and retains both linear and quadratic pieces in the observable. The 48-system previous validation is preserved as an accompanying reference figure; original source scripts are in the Stage 4 archive.

S6. Tangent response under partial synchronization

Let Φ solve $\dot{\Phi} = J(t)\Phi$. A finite kick ϵv applied to a reference trajectory yields $q_{kick}(t) - q_{ref}(t) \simeq \epsilon \nabla q(\theta(t))^{\top} \Phi(t, t_0) v$. The kicked and reference trajectories must use common noise, so that their difference probes the dynamical response rather than independent stochastic fluctuations. This response identity is *not* equivalent to the spontaneous ACF in general non-reversible systems. Ablations of temporal Jacobian order from Stage 5 are included among the reference figures; source files remain available in the Stage 5 research archive.

S7. What belongs to scope rather than the principal claims

Earlier modeling stages explored statistical nulls, independent-noise checks, response-conditioned covariance, and AR/mode-based predictions. These establish provenance and inform model choice, but the manuscript does not claim superior forecasting, novel Mori–Zwanzig identities, universal phase-transition exponents, or brain-imaging validation. The limitations directly relevant to the paired intervention (incomplete r distribution matching; calibration of K; 1/e threshold choice; partial identification of co-varying graph properties) are therefore retained in the main text.

S8. Scope of potential uses and non-equivalence of observable definitions

The observable $q(t)$ is an edge–nonedge contrast of phase coherence, not a BOLD-based static or dynamic structure–function Pearson correlation. Any extension to brain imaging requires an observation model and a separate validation against appropriate covariance-preserving

null systems. Likewise, extension to power-grid analysis requires swing-equation or related electrical-network models, calibrated operating points and physical constraints. The present implications are methodological, not domain-specific experimental claims.

S9. Reference and source audit protocol

The main manuscript includes 60 numbered references covering network synchronization, temporal structure–function coupling, applications, stochastic dynamics and reduced-order modeling.

S10. Earlier independent-noise replication on 256-node networks

An earlier holdout study examined eight degree-sequence-matched Watts–Strogatz graph pairs at $N = 256$ with natural frequencies held the same across the two members of each pair. This ensemble precedes the 30-pair $N = 128$ validation and is not pooled with it for primary statistical inference. The eight-pair mean r was 0.31493 in the original and 0.32021 in the rewired networks. The mean $1/e$ memory of q was 2.05683 versus 1.12524, respectively (original minus rewired: 0.93159). The corresponding residual q memory after contemporaneous *linear* adjustment for r^2 was 1.41984 versus 1.00766 (difference 0.41218). Paired two-sided sign-flip tests gave $p = 0.0078125$ for these temporal-memory contrasts. The older residual adjustment is not the same as the nonlinear lagged adjustment used in the new 30-pair dataset. The earlier independent noise was new relative to calibration, but the graph ensemble and frequency vectors were reused from the exploratory experiment: it is a noise holdout, *not* an independent graph-family validation. See the Stage 3 archived data and code for graph-level details.

S11. Conditional tangent covariance reconstruction in partial synchrony

An earlier Stage 6 investigation provides an independent consistency check that connects spontaneous temporal covariance to conditional response sensitivities. For the stationary diffusion $d X_t = f(X_t)\,dt + \sqrt{2D}\,dW_t$, let $P_t q(x) = E\left[q(X_t) \mid X_0 = x\right]$ and let π denote the stationary distribution. For $T \geq \tau \geq 0$,

$$Cov_\pi\left(q(X_0), q(X_\tau)\right) = 2D \int_\tau^T \left\langle \nabla P_s q, \nabla P_{s-\tau} q \right\rangle_\pi ds + Cov_\pi\left(P_T q, P_{T-\tau} q\right).$$

Under regularity assumptions for differentiating through the stochastic flow, the conditional gradient is the *mean* tangent response, not the sensitivity of a single noise trajectory:

$$\nabla P_s q(x) = E_x\left[\Phi_s^{\top}\, \nabla q(X_s)\right].$$

The identity follows from Markov semigroup covariance relations and the diffusion carré-du-champ; it is not asserted as a new theorem. The numerical implementation used independent conditional-noise branches and a finite-horizon terminal remainder. For three original $N = 24$

graph examples, directly estimated variances of q versus reconstructed variances were: WS 0.03200 versus 0.03042; degree-preserving rewired WS 0.00659 versus 0.00622; ER 0.00501 versus 0.00543. Six additional independently generated graph realizations and lags 0, 1, and 2 were tested in the Stage 6 archive. This calculation should not be conflated with the Stage 5 common-noise kicked-response experiment. The main article mentions it as a supplementary mechanism check because the conditional branching estimator is computationally costly and the validation is limited to small graph sizes.

S12. Analytic identifiability benchmark

The earliest linear stochastic benchmark considered $dX = -\gamma X\,dt + \sqrt{2\gamma}\,C_*^{1/2}\,dW_t$, whose stationary covariance is C_* for all $\gamma > 0$, although its time-lagged covariance is $C(\tau) = e^{-\gamma\tau}C_*$. For a centered quadratic statistic in the isotropic family, the relaxation time is $1/(2\gamma)$. This familiar Ornstein–Uhlenbeck counterexample illustrates why zero-lag covariance is insufficient to identify a temporal relaxation scale; it is motivation, not a novel proof of a phase-transition criterion. Full numerical experiments and scripts are in the Stage 1–2 pilot archive.

Supplementary figure legends

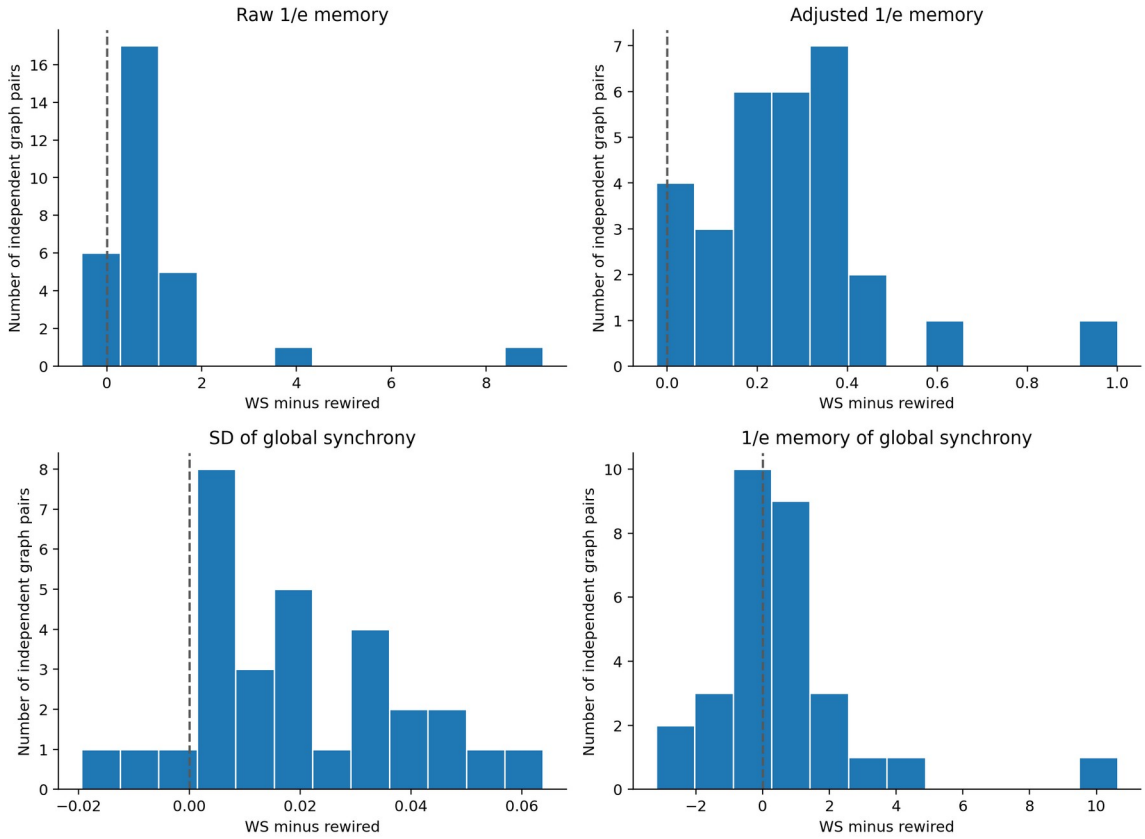


Figure S1. Distribution of graph-level pair differences in raw and adjusted q memory, global order fluctuations and global order memory (original minus rewired). A positive difference indicates greater value in the original Watts–Strogatz graph.

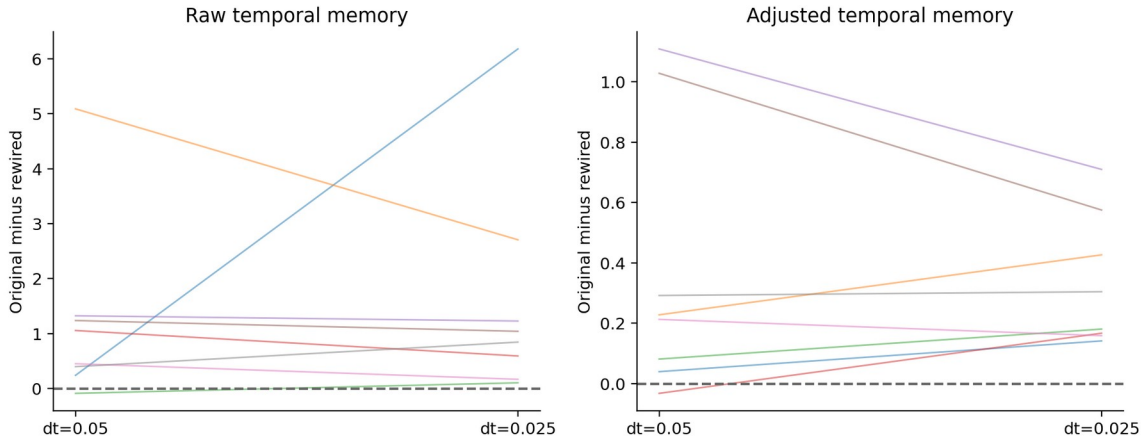


Figure S2. Step-halving check with paired Brownian increments, showing changes in original-minus-rewired raw and adjusted memory for eight graph pairs at $dt = 0.05$ and $dt = 0.025$.

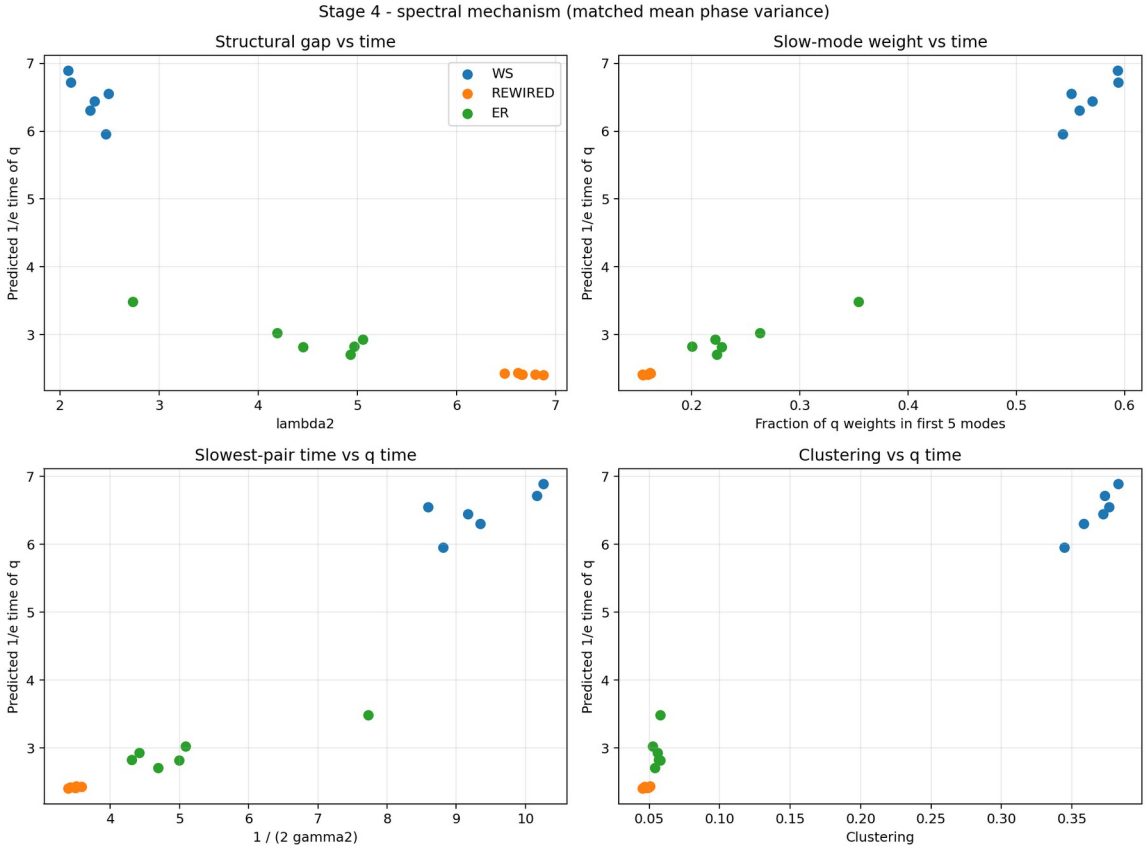


Figure S3. Spectral correlates of the *predicted* near-locking contrast memory across three network families. Unlike main Figure 3, these panels display only predictions and structural diagnostics; no independently measured nonlinear memory values appear in this figure.

Reproducibility records

- data/design_frozen.json: numerical parameters used before result inspection.

- data/paired_graph_design.csv: graph/frequency seeds, graph diagnostics, calibration coupling.
- data/independent_holdout.csv: 120 holdout-condition records, including r and q statistics.
- data/paired_statistics.csv: graph-level estimates, confidence intervals and tests.
- data/K_sensitivity.csv: 36 sensitivity conditions.
- data/step_halving.csv: 32 timestep-check records.
- new_validation.py, numerical_checks.py, make_figures.py: independent validation and plotting scripts.

Funding: No external funding or grant support was received. Author: Yousef Jamali (sole author). Competing interests: The author declares no competing financial or non-financial interests.